Mass Transfer in AC Electrolysis

Part II: Experimental Study on Sinusoidal Current

An experimental study has been made for laminar mass transfer to a rotating disk and a rotating hemispherical electrode when sinusoidal alternating current (AC) together with direct current (DC) are flowing across the electrode/electrolyte interface. A resistor-capacitor circuit was used to measure the phase shift between the applied AC and the resulting periodical concentration overpotential. The limiting AC current density corresponding to a zero instantaneous surface concentration was determined as a function of AC frequency and DC current density. The experimental data agreed with the theoretical calculations in a regime of a dimensionless AC frequency $K = (\omega/\Omega)Sc^{1/3}$ greater than 1 and less than 200.

C. Y. CHENG and D-T. CHIN

Department of Chemical Engineering
Clarkson University
Potsdam, NY 13676

SCOPE

This work is to experimentally contest the film model of Part I for the analysis of laminar mass transport to a rotating disk electrode and a rotating hemispherical electrode when sinusoidal AC together with DC are used for the electrolysis. The reduction of potassium ferricyanide was used for the measurement. A parallel resistor and capacitor circuit was used to determine the phase shift between the applied AC and the resulting periodical concentration overpotential. The limiting AC current densities corresponding to zero surface concentration have been found from the amplitude of AC densities and periodical concentration overpotential curves. The measurement was made for a range of applied DC from 0 to the limiting DC current density ($400 < Re < 30{,}000$) and a dimensionless AC frequency, $K = (\omega/\Omega)Sc^{1/3}$, from 1 to 240.

CONCLUSION AND SIGNIFICANCE

An experimental technique has been developed for studying mass transfer in AC electrolysis with sinusoidal current. The results substantiate the theoretical analysis of Part I based on a film model on the rotating hemispherical electrode. The experimental limiting AC current densities agreed with the theoretical predictions to within ± 4.3% over a range of dimensionless AC frequencies, $K = (\omega/\Omega)Sc^{1/3}$ from 1 to 200, and superimposed DC from 0 to the limiting DC current density. The measurement of a phase shift between the applied sinusoidal AC and the periodical component of the resulting concentration overpotential agreed with the theory to within ±6% for K varying from 1 to 50.

INTRODUCTION

Alternating current has an interesting effect on electrode processes: it reduces the electrode potential, destroys the electrochemical passivity, and accelerates the corrosion of the metals (Venkatesh, 1979; Chin, 1979a,b). These phenomena can be attributed to the fact that AC produces periodic concentration changes at the electrode surface. The resulting concentration overpotential depends not only on the magnitude of the AC current density but also on the AC frequency (Warburg, 1899, 1901).

In Part I, we made a theoretical analysis of the concentration changes of a reacting species when sinusoidal AC together with direct current were flowing across the surface of a rotating hemispherical electrode. Numerical results were presented for the limiting AC current densities corresponding to zero concentration on the electrode surface in laminar flow. The resulting AC concentration overpotential and the phase shift between AC and the overpotential were also examined.

The main objective of this study is to experimentally test the theoretical calculations of Part I. A rotating disk electrode (RDE) and a rotating hemispherical electrode (RHE) were used for the mass transfer measurement when the electrodes were galvanostatically polarized with a DC superimposed with a sinusoidal AC. The concentration overpotential variations and the phase shift between AC and the overpotential wave were measured with a resistor-capacitor (R-C) circuit. The limiting AC current density was determined for various AC frequencies and DC current densities.

EXPERIMENTAL

Electrode and Cell Arrangement

Two electrodes were used for the experimental investigations. The first was a platinum rotating disk electrode (Pine Instrument DT6), whose radius and surface area were 0.382 cm and 0.458 cm^2, respectively. The second electrode was a gold-plated rotating hemispherical electrode mounted on a Teflon cylinderical support of an equal radius. The radius of the hemispherical electrode was 0.95 cm. The support rods for both electrodes were machined to fit into the spindle shaft of a high-speed rotator (Pine Instrument ASR2). The rotator had a speed range of 0–10,000 rpm. A silver-carbon slip-ring contact on the rotator was used for the electrical connection to the platinum disk and gold hemispherical electrodes.

The cell arrangement is shown schematically in Figure 1. The radius and

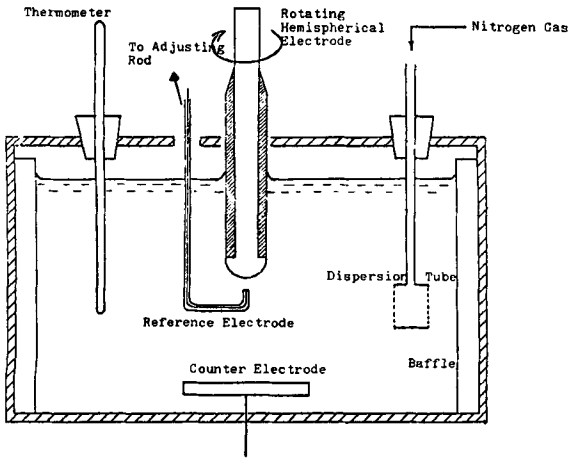

Figure 1. Cell arrangement.

the height of the cell were 7.62 cm and 15.24 cm, respectively. A nickel sheet embedded in an epoxy block and located at the bottom of the cell was used as the counterelectrode. The reference electrode was a platinum wire inserted in a glass tube which was mounted on an adjusting rod on the cell cover. The axial and the lateral distance between the reference and the working electrodes could be varied by adjusting the axial and lateral micrometer heads. A polyethylene tube was used for bubbling nitrogen gas.

Reduction of ferricyanide ion on the working electrode was used for the mass transfer measurement. The electrolyte was composed of 0.01 M potassium ferricyanide, 0.1 M potassium ferrocyanide and 1 M sodium hydroxide. The solution was prepared by dissolving Baker analyzed chemicals in distilled water. The concentration of ferricyanide ion was determined by an iodometric titration. The specific gravity and viscosity of the electrolyte were 1.06 g/cm^3 and 0.0114 g/cm-s, respectively at 23°C.

Electrical Circuit

The electrical circuit is shown in Figure 2. A potentiostat (Wenking LT78) operated on the galvanostatic mode was used to supply constant currents. The DC current was measured with a multimeter (Hewlett 3465B) across a precision resistor, R_2 (100 Ω), connected in parallel with a capacitor, C_1 (11,200 μF). The super-imposed AC was supplied to the potentiostat from an AC signal generator (Hewlett 2311A). The value of AC current was precisely adjusted by connecting a 1,000 Ω potentiometer, R_5, to the AC signal generator and was measured by a multimeter across a precision resistor, R_1 (10 Ω). The root mean square (*rms*) of the resulting periodic component of potential changes between the working and the reference electrode was measured by a multimeter (Hewlett 3466); its waveform was observed on one channel of a dual-trace oscilloscope (Tektronix 214). A switch *S* was used to alternate the experimental measurements. For the limiting AC current density measurement, switch *S* was set on position 1, and the current was determined by measuring the voltage drop across a precision resistor, R_4 (10 Ω). For the phase-shift measurement, the switch *S* was set on position 2 and the current passed a parallel arrangement of a variable resistor, R_3 (0–11,125 Ω), and a precision capacitor, C_2 (12 μF). The waveform of the applied AC was observed on the second channel of the oscilloscope. The resistor-capacitor circuit was used to compensate for a phase lag between the applied AC and the resulting periodic overpotential waves. When the resistor, R_3, was adjusted to make the AC and the resulting overpotential be in the same phase, the oscillogram would show a straight line on the $X - Y$ mode. In this way, the phase shift between the two waves was determined.

Procedures

Before each run, the working electrode was cleaned with methonol and was cathodically treated at −3.0 V for 2 minutes in 1 N NaOH solution followed by rinsing in distilled water. The clean electrode was transferred quickly into the solution and installed in the rotator assembly. To avoid a possible secondary reaction due to the reduction of dissolved oxygen, high-purity nitrogen was passed through the electrolyte before each run and passed over the electrolyte during the run.

The rotating disk electrode was used first. The reference electrode was locatead in the middle of the working electrode and 1 mm away from the electrode surface. The experiment began with the determination of the limiting DC current density for the reduction of ferricyanide ion. The sinusoidal AC (10–1,000 Hz) together with DC were then applied to the cell. The root mean square of the periodic concentration overpotential and the phase shift between the AC and the potential were measured over a range of rotational speeds from 300 to 3,600 rpm. Then the rotating hemispherical electrode was used as the working electrode. The position of the reference was varied from the pole ($\theta = 0°$) to the equator ($\theta = 90°$). The diffusion limited DC currents, the periodic concentration overpotentials, and the phase shift between AC and the resulting potential waves were also measured. All experiments were performed at a constant temperature of 23 ± 1°C.

RESULTS AND DISCUSSION

Phase-Shift Measurement

Figure 3 is an oscillogram illustrating how the phase shift between the applied AC and the resulting periodic concentration overpotential was determined. In Figure 3a, the AC waveform (dashed curve) was not in phase with the periodic potential (solid curve); thus the corresponding oscillogram on an *X*-*Y* scale (the horizontal axis, *X*, was the AC potential and the vertical axis, *Y*, was the AC current) exhibited an elliptical shape in Figure 3b. The R-C circuit was used to compensate for the phase lag to make AC in phase with the resulting concentration overpotential, Figure 3c.

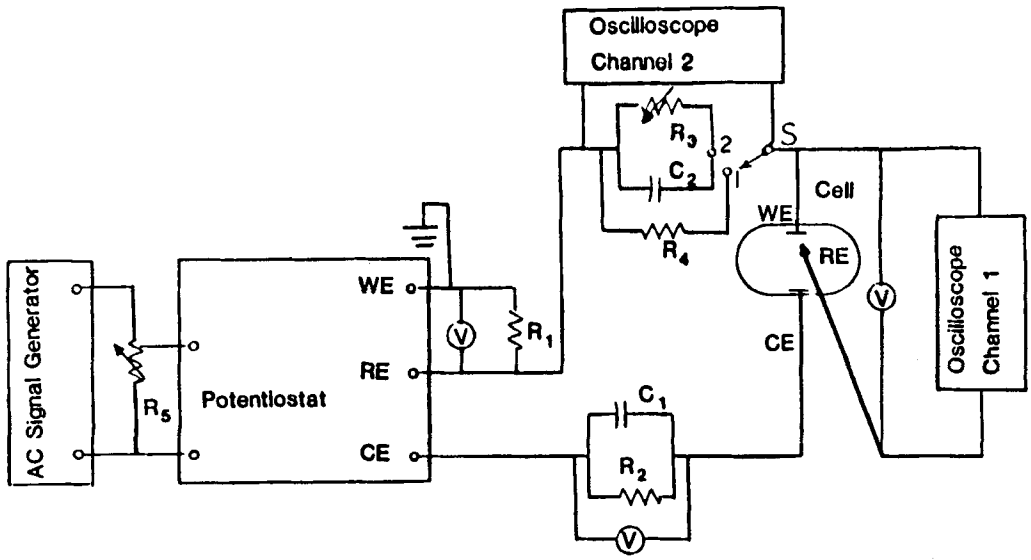

Figure 2. Electrical circuit: *WE*, working electrode; *RE*, reference electrode; *CE*, counterelectrode; *S*, switch; *V*, multimeter. The values of resistors and capacitors are: $R_1 = 10$ Ω; $R_2 = 100$ Ω; $R_4 = 10$ Ω; $0 \leq R_5 \leq 1{,}000$ Ω; $C_1 = 1{,}120$ μF; $C_2 =$ μF; $0 \leq R_3 \leq 11{,}125$ Ω.

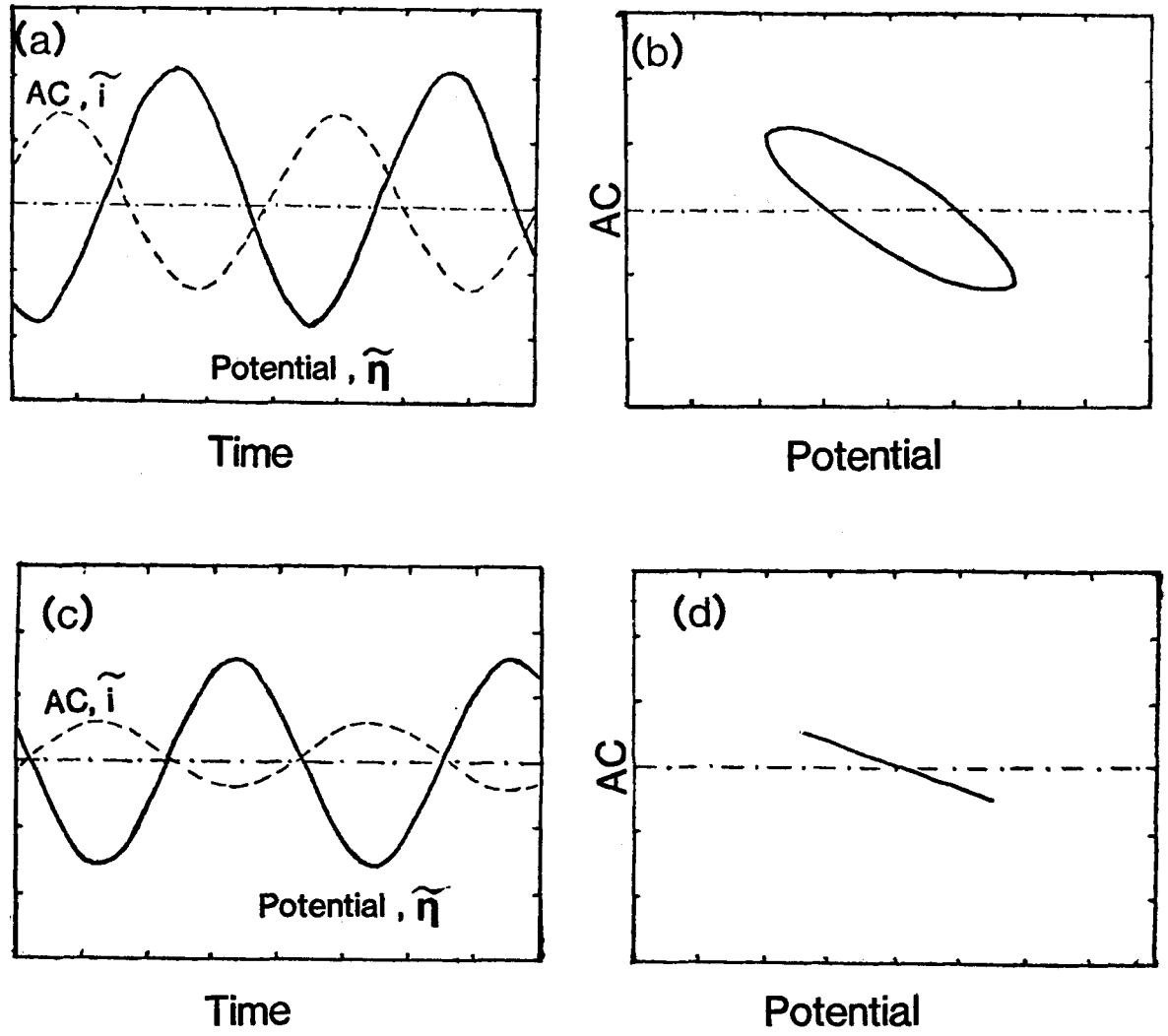

Figure 3. Oscillogram for the phase-shift measurement: (a) waveforms for the applied AC, $\tilde{i}$, and the periodical concentration overpotential without phase compensation; (b) corresponding oscillogram in the *X-Y* mode; (c) waveforms of the applied AC and the periodical concentration overpotential after phase compensation; and (d) corresponding oscillogram in the *X-Y* mode. Time scale in (a) and (c): 12.5 ms/div. Potential scale: 25 mV/div. Current scale: 6.25 mA/div.

(Figure 3c actually shows that the two waves were 180° out of phase due to the design of the electrical circuit to use a common ground connection to the oscilloscope.) Figure 3d shows the corresponding oscillogram on the *X-Y* mode which became a straight line when the two waves were in phase. The values of the phase shift, Δ_s, were calculated by the relationship:

$$\Delta_s = \tan^{-1} \omega C_2 R_3 \qquad (1)$$

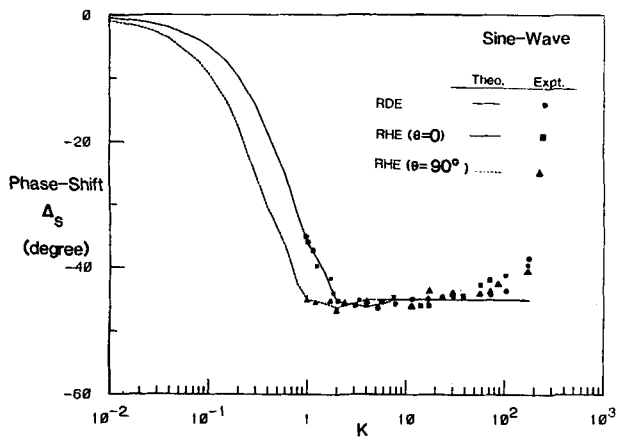

Figure 4. Phase shift between the applied AC and the resulting overpotential at various *K* for the RDE and the RHE at $\theta = 0°$ and 90°.

where ω is the AC frequency, C_2 is the precision capacitance and R_3 is the resistance of the variable resistor in the R-C circuit.

Figure 4 shows the results of phase-shift measurements for the rotating disk and the rotating hemispherical electrodes at two positions of the reference electrode ($\theta = 0°$ and $\theta = 90°$). The symbols, ●, ■, and ▲ are the present experimental data. The solid line represents the theoretical calculations of Part I for the RDE and RHE at $\theta = 0°$, and the dash line is the theoretical calculations for the RHE at $\theta = 90°$. There was a good agreement between theory and experimental data for $K < 50$. The maximum deviation in this regime was ±6%. The results also indicate that, when K was greater than 2, the phase shift became independent of position on the RHE. As K became greater than 50, the deviation increased. This was due to the experimental difficulty that the periodic concentration overpotential component became smaller at high AC frequency (less than 1 mV at 200 Hz) and electrical noise interferred with the measurement.

Limiting AC Current Density

Figure 5 shows that the root mean square of periodic component of the concentration overpotential for RHE at two positions of the reference electrode ($\theta = 0°$ and $\theta = 90°$). The measurements were made for a range of dimensionless AC frequency, K, from 2 to 30 with the DC current density, i, equal to zero. The data are plotted in the figure as a function of the amplitude of the applied AC, i_p, normalized by the experimental limiting DC current density on

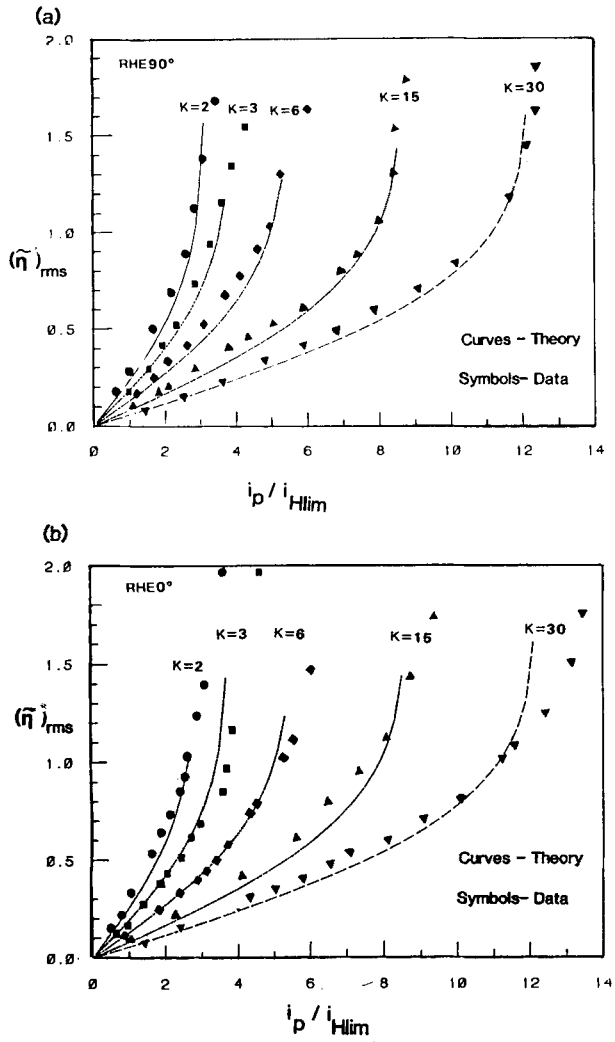

Figure 5. Periodical concentration overpotential at the RHE as a function of the amplitude of the applied AC for K = 2,3,6,15,30. The position of the reference electrode was (a) 90° and (b) 0°.

the RHE, $i_{H\text{lim}}$. For comparison, the theoretical predictions of the rms of the periodic concentration overpotential from the analysis of Part I are also given in the figure as the curves. For the theoretical curves, the horizontal axis was normalized by an $i_{H\text{lim}}$ calculated from the expression (Newman, 1972):

$$i_{H\text{lim}} = 0.45\, nFD^{2/3}C_\infty \nu^{-1/6}\Omega^{1/2} \qquad (2)$$

The results indicate that the *rms* of the periodic overpotential component, $(\tilde{\eta}^*)_{rms}$ increased with increasing AC current density, $i_p/i_{H\text{lim}}$, and decreased with increasing AC frequency K. When the amplitude of AC, i_p, approached to the limiting AC current density, $i_{p\text{lim}}$, the minimum of the surface concentration wave became zero. Then, in theory, the value of $(\tilde{\eta}^*)_{rms}$ would jump to an infinite value as shown by the theoretical curves in the figure. However, the transition for the experimental $(\tilde{\eta}^*)_{rms}$ values were not as sharp as the theoretical curves; the deviation was caused by the occurrence of a secondary reaction (hydrogen evolution) in the electrolytic system. The agreement was better at the equator (θ = 90°) than at the pole (θ = 0°). This could be attributed to the fact that the zero surface concentration occurred first at the equator of the RHE of Part I.

Figure 6 shows two experimental methods for the determination of the limiting AC current density. The data in the figure were obtained with a rotating disk electrode (K = 6 and $\bar{i}$ = 0), and the AC amplitude in the figure has been normalized with a limiting DC current density, $i_{D\text{lim}}$, on the disk electrode:

$$i_{D\text{lim}} = 0.62\, nFD^{2/3}C_\infty \nu^{-1/6}\Omega^{1/2} \qquad (3)$$

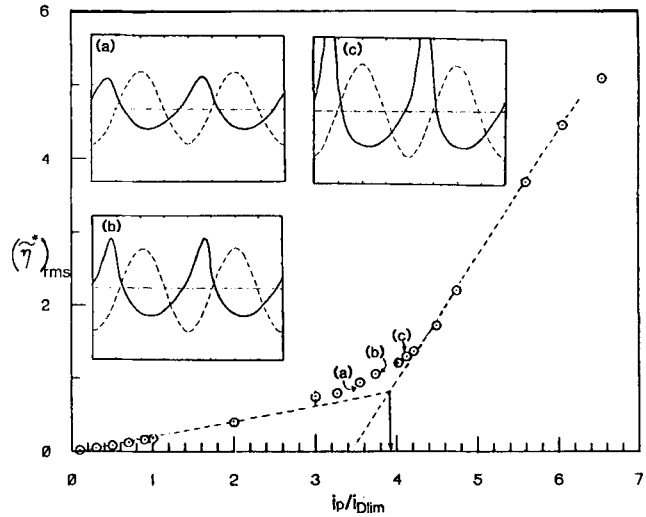

Figure 6. Periodical concentration overpotential at the RDE as a function of the amplitude of applied AC for K = 6 and $\bar{i}$ = 0. The oscillograms of applied AC and potential waves at the data points a,b,c, are given in insets (a), (b) and (c). The scales for the oscillogram are the same as in Figure 3.

In the first method the *rms* of the periodic component of the overpotential changes was plotted against $i_p/i_{D\text{lim}}$. The data exhibited two linear regimens, and the values of i_p at the point of intersection of the two straight lines was taken as the limiting AC current density, $i_{p\text{lim}}$. The value of $i_p/i_{D\text{lim}}$ (K = 6, and $\bar{i}$ = 0) determined this way was 3.92, which agreed with the theoretical value of 3.974 of Part I to within 1.5%. The second method was to follow the oscilloscope traces of the overpotential responses, Figure 6a-c. The oscillogram in Figure 6a corresponds to $i_p/i_{D\text{lim}}$ = 3.6; at this value, the resulting concentration overpotential (solid line) was only slightly distorted from the sinusoidal shape. As $i_p/i_{D\text{lim}}$ increased to 3.8, the negative peak of the potential wave became narrower and steeper. As $i_p/i_{D\text{lim}}$ increased to 4.2, the peak became so large that it was out of range on the oscilloscope screen. Thus, the shape of the oscillograms could also be used to find experimental value of the limiting AC current density. Both methods were satisfactory and agreed with each other to within ±2%. In this way, the limiting AC current densities on the RDE and RHE were experimentally determined for a range of AC frequency from 0 to 1,000 Hz, DC current densities from 0 to the limiting DC current density and speed of rotation from 300 to 3,600 rpm ($400 < RE < 30{,}000$).

Figure 7 shows the results of the limiting AC current density on the RDE, $i_{p\text{lim}}/i_{D\text{lim}}$ as a function of the dimensionless AC frequency. The parameter in the figure are the superimposed DC current density, $\bar{i}$, normalized by the limiting DC current density on the disk electrode $i_{D\text{lim}}$. For comparison, the theoretical predictions from the previous analysis using a film model (Part I) are

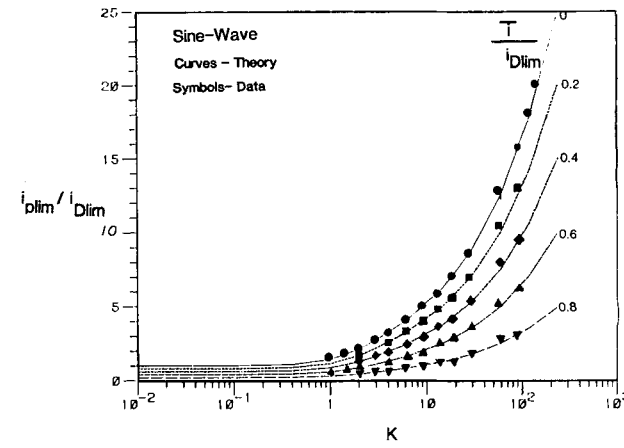

Figure 7. Limiting AC current density on the RDE as a function of K for various applied DC current densities $\bar{i}/i_{D\text{lim}}$.

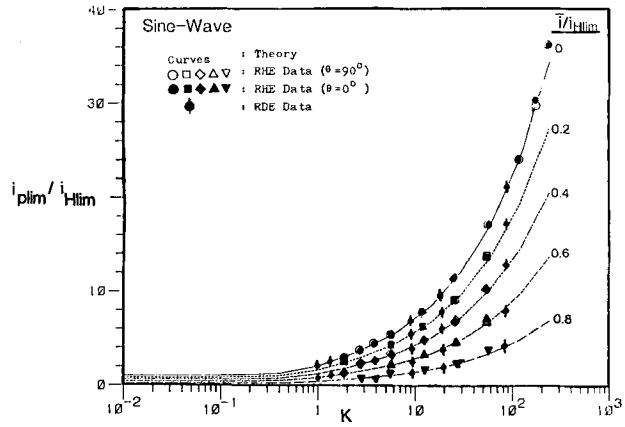

Figure 8. Limiting AC current density on the RHE as a function of K for various applied DC current densities, $\bar{i}/i_{Hlim}$. For comparison, some of the RDE data are also plotted in the figure as Φ.

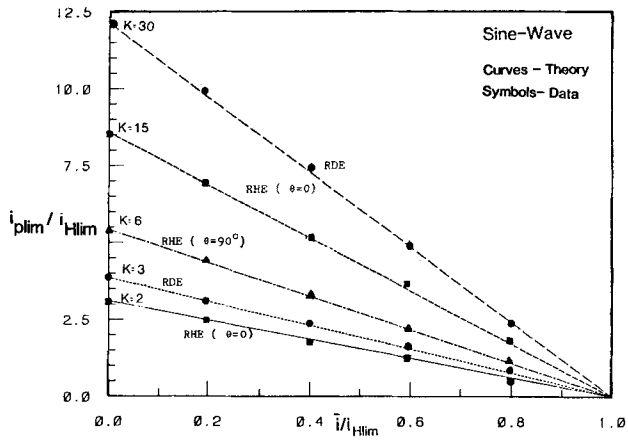

Figure 9. Limiting AC current densities as a function of the applied DC current density.

also plotted in the figure. The limiting AC current density increased with increasing K, and decreased with increasing DC current $\bar{i}$. The experimental results agreed with the model very well. The maximum deviation occurring at $K = 180$ was 4.3%.

The results for the limiting AC current density on the RHE are given in Figure 8, where i_{plim}/i_{Hlim} are plotted against K for a range of $\bar{i}/i_{Hlim}$ from 0 to 0.8. Again, the experimental data fit the previous theoretical model to within ±6.1%. The position of the reference electrode on the RHE surface did not affect the measurement. Also, if the AC-limiting current on the RDE is normalized by the limiting DC current density on the RHE, i_{Hlim}, the data falls on the RHE curves, Figure 8. This implies that the theoretical model for RHE is applicable to the RDE by setting $\theta = 0°$.

The data in Figures 7–8 are replotted in Figure 9 in the form of i_{plim}/i_{Hlim} vs. $\bar{i}/i_{Hlim}$ with the dimensionless frequency K as the parameter. The figure indicates that the limiting AC current density was a linear function of applied DC current density. The limiting AC current density decreased with increasing DC, and became zero when DC was equal to the limiting DC current on the electrode.

ACKNOWLEDGMENT

The Donors of the Petroleum Research Fund, administered by the American Chemical Society, are acknowledged for support of this research. We would also like to thank I-Yuan Wei of AMP Inc., Harrisburg, PA, for his help in the preparation of a gold-plated rotating hemispherical electrode.

NOTATION

a = radius of the working electrode, m
C_i = capacitance, (i = 1,2), F
C = bulk concentration, kmol/m^3
D = diffusivity, m^2/s
F = Faraday constant, 9.65×10^7 C/kg equiv.
$\bar{i}$ = applied DC current density, A/m^2
$\tilde{i}$ = applied AC current density, A/m^2
i_{Dlim} = limiting DC current density for RDE, A/m^2
i_{Hlin} = limiting DC current density for RHE, A/m^2
i_p = amplitude of AC current density, A/m^2
i_{plim} = limiting AC current density, A/m^2
K = dimensionless AC frequency, $K = \left(\frac{\omega}{\Omega}\right) Sc^{1/3}$
n = number of electrons, kg equiv./kmol
R = gas constant, J/kmol·K
Re = Reynolds number, $\frac{a\Omega^2}{\nu}$, dimensionless
R_i = resistance (i = 1,2,3,4,5), Ω
Sc = Schmidt number, $Sc = \nu/D$, dimensionless
T = temperature, K

Greek Letters

Δ_s = phase shift between AC and $\tilde{\eta}$, rad
θ = Meridional coordinate of RHE, rad
$\tilde{\eta}$ = periodical component of the concentration overpotential, V
$(\tilde{\eta}^*)_{rms}$ = root mean square of the dimensionless periodical concentration overpotential $\tilde{\eta}^* = \tilde{\eta}\frac{nF}{RT}$, dimensionless
ν = kinematic viscosity, m^2/s
ω = AC frequency, rad/s
Ω = rotating speed, rad/s

Subscripts

Dlim = limiting value of RDE
Hlim = limiting value of RHE
lim = limiting value
rms = root mean square
p = amplitude
∞ = bulk value

Superscript

* = dimensionless value

Other Symbols

- = DC component
~ = AC component

LITERATURE CITED

Cheng, C. Y., and D-T Chin, "Mass Transfer in AC Electrolysis," Part I, *AIChE J.*, **30**, (Sept., 1984).

Chin, D-T, and T-W Fu, "Corrosion by Alternating Current: A Study of the Anodic Polarization of the Mild Steel in Na_2SO_4 Solution," *Corrosion*, **35**(11), 514 (1979a).

Chin, D-T, and S. Venkatesh, "A Study of Alternating Voltage Modulation of the Mild Steel," *J. Electrochem. Soc.*, **126**, 1908 (1979b).

Newman, J., "Mass Transfer to a Rotating Sphere at High Schmidt Numbers," *J. Electrochem. Soc.*, **119**, 69 (1972).

Venkatesh, S., and D-T Chin, "The Alternating Current Electrode Process," *Isr. J. Chem.*, **18**, 56 (1979).

Warburg, E., "Ueber das Verhalten sogenannter unpolarisirbayer Elktroden gegen Wechselstron," *Ann. Physik*, **67**, 493 (1899).

Warburg, E., "Ueber die Polarisationscapacitat des Platins," *Ann. Physik*, **6**, 125 (1901).

Manuscript received May 2, 1983; revision received August 18, and accepted August 21, 1983.